Dissecting the aerodynamics of *Morpho* butterly flight using various turbulence models

Dario Amadori, Jaap Windt, Camille Le Roy, Florian Muijres

September 15, 2019

1 Introduction and main objective

Morpho butterflies are among the largest flying insects, boasting a wing that can reach 20 centimetres in span. Such characteristic allows these butterflies to perform flying techniques that are common in birds but not in insects, like the gliding and flap-gliding flight style. During flap-gliding, *Morpho* butterlies fly at speeds of approximately 1.5 m s^{-1}, and thus the wings operate at Reynolds numbers of the order of 10^4. At this transitional Reynolds number regime, aerodynamic performance of a wing is notoriously difficult to estimate, as turbulence state is difficult to determine *a priori* (Spedding et al. [2008]). Here, we model the aerodynamics of gliding *Morpho* butterflies using different turbulence models with the aim at understanding which ones can give more realistic and reliable results.

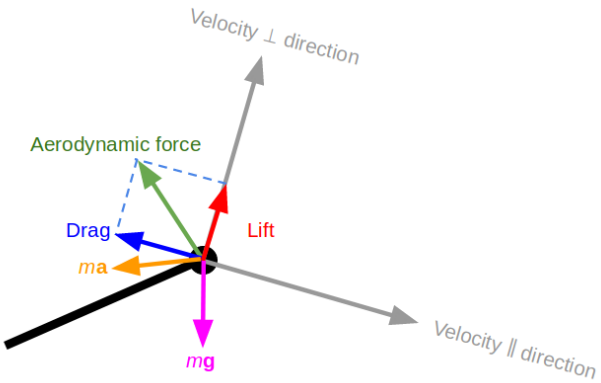

Fig. 1: Free body diagram of a gliding butterfly, including vectors normal and parallel to the flight direction, body acceleration vector and vectors of all external force acting on the animal. The animal is depicted as a lolly-pop whereby the circle is the head. The total aerodynamic force consists of lift and drag components, whereby drag is parallel to the velocity vector. Applying Newton's second law of motion to this system, lift and drag can be estimated from the acceleration and weight vectors (Eq. 1).

2 Kinematics and morphology of a flap-gliding *Morpho* butterfly

The experimental data used for validating our numerical simulations is a glide section of a flap-gliding flight of a *Morpho cisseis* butterfly. The flight was filmed in semi-field conditions with a stereoscopic high-speed camera system, recording at 240 frames per second. Throughout the stereoscopic video, we tracked the position of head, tail, and left and right wingtips, using a manual tracking program. Based on the head location data, we estimated the velocity (**v**) and acceleration (**a**) of the animal throughout the glide (Figure 2 (a)); by combining the wing orientation data with the velocity data, we determined the angle-of-attack of both wings throughout the gliding flight (Figure 2 (b)).

Butterfly wings consist of a front and hind wing, that are most of the time pressed against each other, and thus effectively operate as a single wing. Each wing consists of a flexible membrane (~0.1 mm thick) supported by stiffeners (~1mm thick). These stiffeners, called wing vanes, are mostly allocated near the leading edge. The wing surface is covered by scales that give colour to the wing, but also produce roughness on the wing surface. The wing of a *Morpho cisseis* butterfly has an average width of 7.5 cm and a mean chord length of 5.2 cm.

3 Inverse dynamics model of a gliding butterfly

Based on the accelerations of the butterfly throughout its gliding flight, we used rigid-body inverse dynamics modelling to estimate the aerodynamic lift **L** and drag **D** acting on the animal (Figure 1). By assuming zero wind conditions, we determined the aerodynamic force ($\mathbf{F}_{\text{aero}}$) acting on the animal using Newton's second law of motion as

$$\mathbf{F}_{\text{aero}} = -m\mathbf{g} + m\mathbf{a}, \tag{1}$$

where m is the mass of the butterfly and **g** is the gravitational acceleration. The next step consists in pulling the drag and lift vectors out of the $\mathbf{F}_{\text{aero}}$ vector. The drag is defined as the aerodynamic force component in the free-stream airflow direction, and is thus calculated as (Figure 2 (c))

$$\mathbf{D} = < \hat{\mathbf{v}}, \mathbf{F}_{\text{aero}} > \hat{\mathbf{v}}, \tag{2}$$

where $\hat{\mathbf{v}}$ the normalised velocity field vector and $< \hat{\mathbf{v}}, \mathbf{F}_{\text{aero}} >$ is the scalar product of $\hat{\mathbf{v}}$ and $\mathbf{F}_{aero}$. Note that this will lead to negative values for drag. The lift was estimated as the difference between the total aerodynamic force and drag as (Figure 2 (d))

$$\mathbf{L} = \mathbf{F}_{\text{aero}} - \mathbf{D}. \tag{3}$$

Finally, based on these results, the lift-to-drag ratio (L/D) throughout the glide phase was determined (Figure 2 (e)).

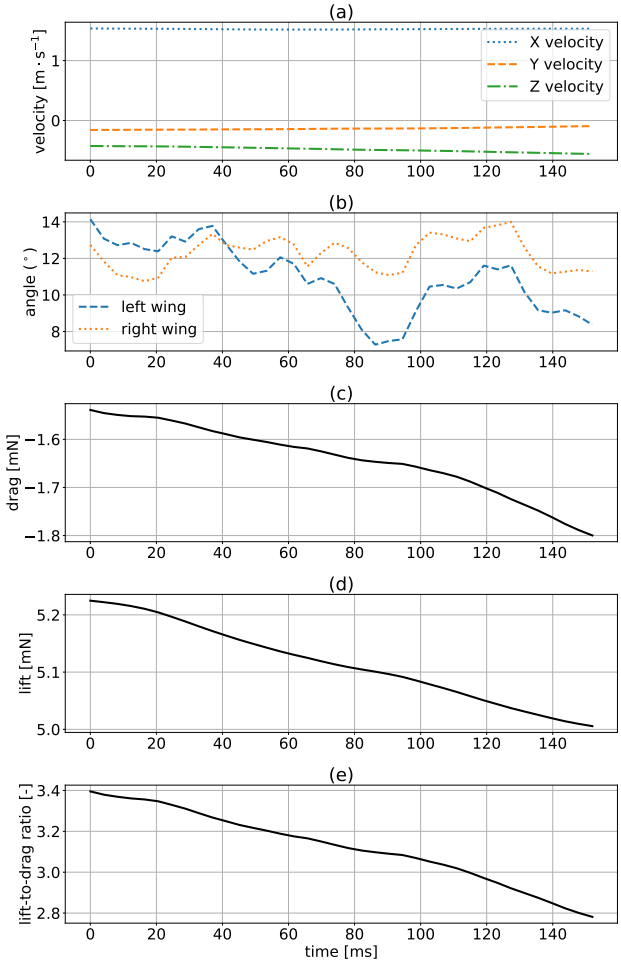

Fig. 2: Experimental kinematics data of the gliding phase in a flap-gliding flight of a *Morpho cisseis* butterfly, determined using stereoscopic high-speed videography and inverse dynamics modelling (Section 3). The parameters shown are the temporal dynamics of flight velocity (a), angle of attack of the left and right wings (b), drag force (c), lift force (d), lift-to-drag ratio (e).

4 Numerical simulation setup

For the numerical simulations, we modelled a single *Morpho* butterfly wing in gliding conditions, whereby the wing root was positioned at a symmetry plane (Figure 3). The wing model consisted of a 1 mm thick rigid smooth flat plate operating at the average angle of attack (10.91°) and average flight speed (1.61m/s) of the digitised gliding flight (Figure 2 (a), (b)). The wing outline was accurately traced from a museum specimen of a *Morpho cisseis* butterfly; the front and hind wing were rigidly connected matching the position that was observed to be used by this specie during gliding flight. The edges of the wing were rounded with 0.5mm radius, except for the edge lying on the symmetry plane, which was sharply cut.

The domain of the numerical simulations consisted of a $2 \times 1 \times 2$ metres box, with the hinge of the wing positioned in the origin, which raises in the middle of the xz plane. An inflow condition directed in the $-x$ direction was set on the boundary plane $x = 1$ and a symmetry condition was set on the boundary plane $y = 0$. All the other external surfaces were defined by a zero-pressure condition and the wing was defined by a no-slip condition.

In order to perform a study on the uncertainty due to spatial discretization, for each case four unstructured grids with different refinement were used (Table 1). The time step was set to 0.8 ms; with this value, the mean flow needs more than 50 time steps to sweep the length of the wing.

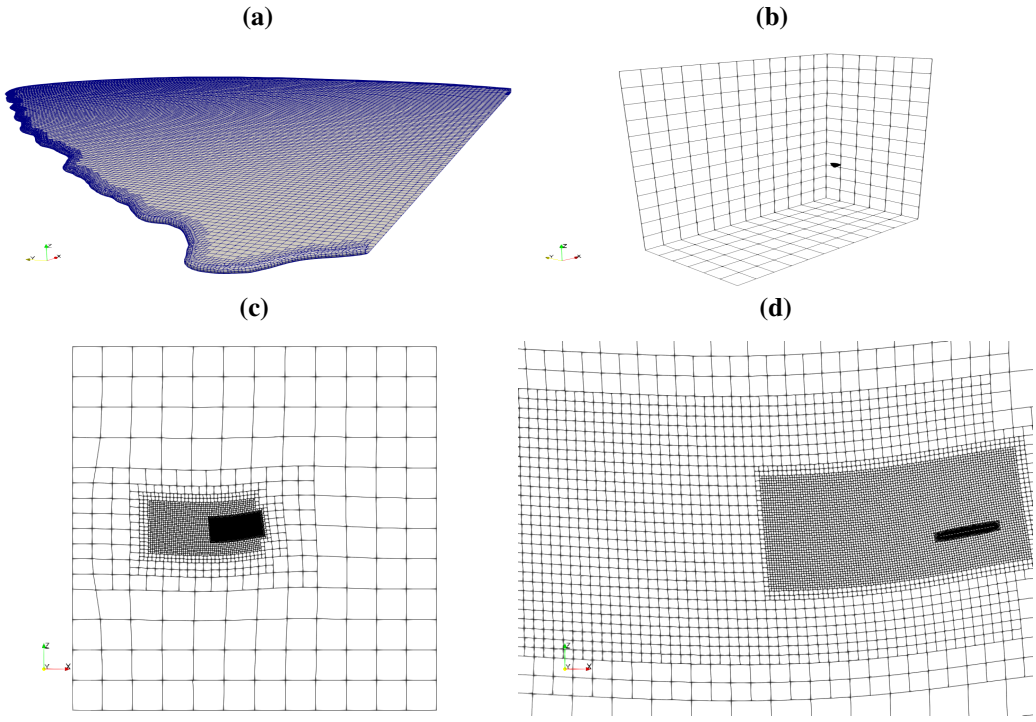

Fig. 3: The mesh topology used for the simulations. (a) the wing surface mesh; (b) the complete computational domain with in its centre the wing surface mesh from (a); (c) the complete symmetry plane, with two box refinements around the wing; (d) zoomed in view of the refinement boxes around the wing, whereby the wing is positioned in the finest cell box.

For this study, we selected five different numerical setups to test, using the following turbulence models: Spalart-Allmaras, SST $\kappa - \omega$, SST $\kappa - \omega$ with $\gamma - \mathrm{Re}_\theta$ transition modelling (with two different inlet conditions: $\nu_t/\nu = 2.5$ and $\nu_t/\nu = 10$) and PANS.

The SST $\kappa - \omega$ model was chosen because it tends to provide relatively precise results, particularly in aerodynamic applications (Menter [1993]); since previous studies suggested that insect flight is characterised by unsteadiness of the flow (Sane [2003]), the steady results obtained with this setup left some doubts. For this reason, we believed that, thanks to its origin and field of application, the Spalart-Allmaras model was as a valid alternative turbulent model to check if any differences would have arisen (Spalart and Allmaras [1992]). Moreover, since it was not possible to state *a priori* if and how turbulence would have been developed, we added to the SST $\kappa - \omega$ model the $\gamma - \mathrm{Re}_\theta$ equations to investigate this topic. Since, following Menter et al. [2004], the latter provided to be sensitive to the inlet conditions imposed, two configurations of the $\gamma - \mathrm{Re}_\theta$ model where set to further investigate this aspect (see validation examples in Langtry and Menter [2005]). Finally, PANS model was chosen as a final attempt to further study this case and to better catch the effects of turbulence. The latter simulations are still in progress and will need further refinements both in time and space to provide reliable data.

5 Results

To test our different numerical cases, we compared the lift, drag and lift-to-drag ratio from the numerical simulations with those estimated from the glide kinematics (Figure 7). The error bars in Figure 7 represent the uncertainties due to spatial discretisation for drag, lift and lift-to-drag ratio for each numerical simulation, which are estimated following the procedure explained in Eça and Hoekstra [2014]. All the uncertainties lie in between 2% and 12%; the estimation is not studied yet for the PANS simulations and not given for the experimental data.

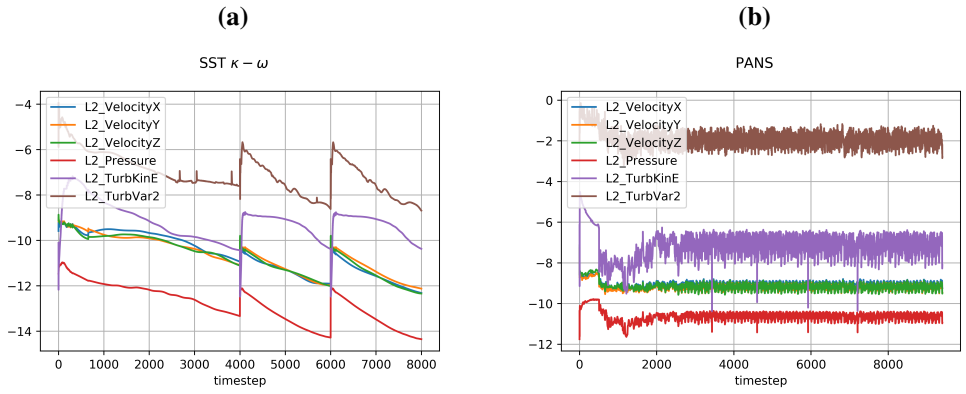

Fig. 4: (a) L_2 norm residuals for the SST κ – omega model with the finest grid, in logarithmic scale; on the x axis the number of time steps. The Spalart-Allmaras and SST $\kappa - \omega$ with $\gamma - \mathrm{Re}_\theta$ transition model have a very similar residuals trend; (b) L_2 norm residuals for the finest grid PANS simulation, in logarithmic scale; on the x axis the number of iterations.

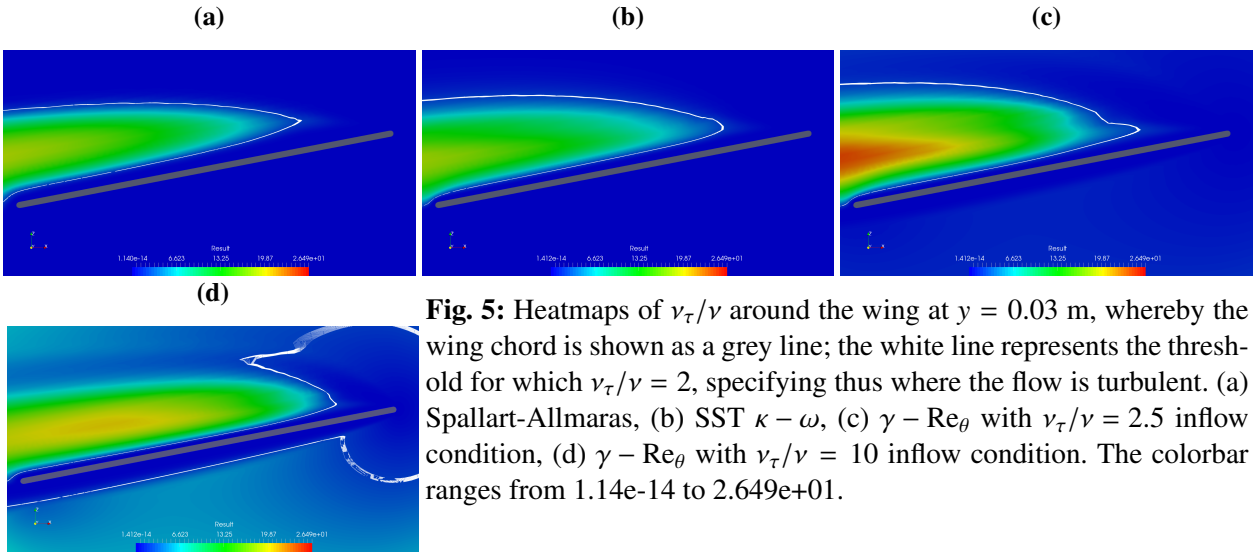

Fig. 5: Heatmaps of ν_τ/ν around the wing at $y = 0.03$ m, whereby the wing chord is shown as a grey line; the white line represents the threshold for which $\nu_\tau/\nu = 2$, specifying thus where the flow is turbulent. (a) Spallart-Allmaras, (b) SST $\kappa - \omega$, (c) $\gamma - \mathrm{Re}_\theta$ with $\nu_\tau/\nu = 2.5$ inflow condition, (d) $\gamma - \mathrm{Re}_\theta$ with $\nu_\tau/\nu = 10$ inflow condition. The colorbar ranges from 1.14e-14 to 2.649e+01.

The SST $\kappa - \omega$, Spalart-Allmaras and SST $\kappa - \omega$ $\gamma - Re_\theta$ simulations converge to a steady flow solution, with L_2-norm residuals reaching values of the order of 10^{-9} (Figure 4a). Due to computational cost restrictions, PANS simulations were run with higher tolerance on the residuals (Figure 4b).

The $\kappa - \omega$, Spallart-Allmaras and $\gamma - Re_\theta$ with both $\nu_\tau/\nu = 10$ and $\nu_\tau/\nu = 2.5$ inflow have a steady flow as result. The PANS simulations lead to unsteady flow configurations, with the first three levels of refinement reaching a periodic state (Figure 8).

Table 1: Number of cells of the four grids used for each turbulence model.

1lev	1,157,340
2lev	3,785,147
3lev	8,406,881
4lev	15,738,960

6 Discussion

Our comparison of aerodynamic forces between the experiment and simulations (Figure 7) shows that all numerical simulations predict larger (in magnitude) drag, lift and lift-to-drag ratio. This systematic offset between experiments and simulations could come from the presence of air currents during the recorded flight, which we assumed to be zero. The experiments were performed in semi-field conditions, so air currents could not be fully controlled, and because butterflies have exceptionally low wing loading small air currents can have a large effect on their flight.

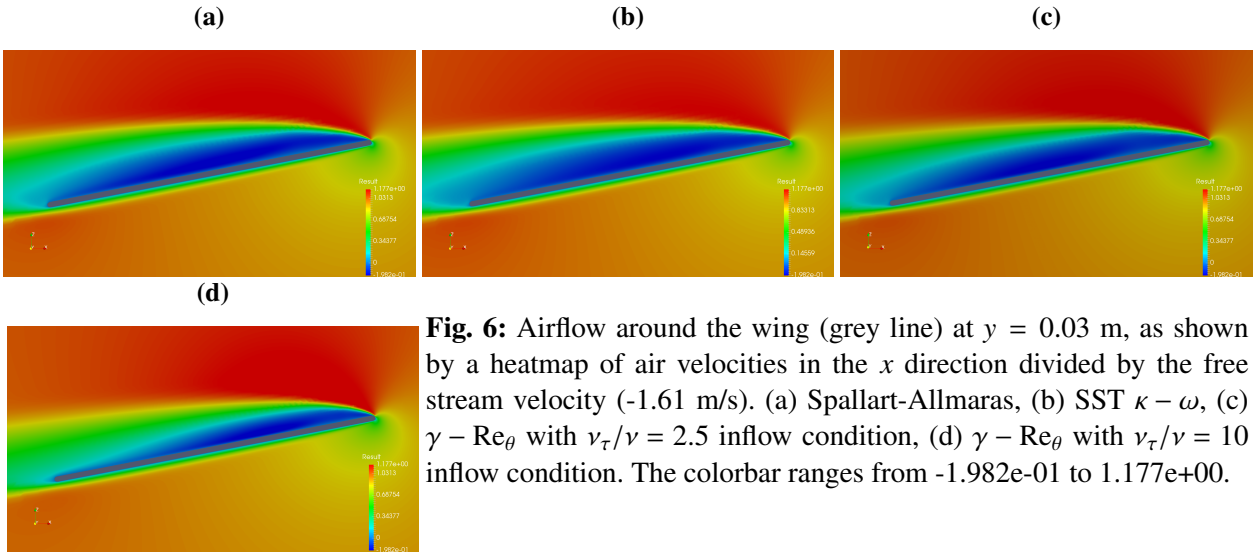

Fig. 6: Airflow around the wing (grey line) at $y = 0.03$ m, as shown by a heatmap of air velocities in the x direction divided by the free stream velocity (-1.61 m/s). (a) Spallart-Allmaras, (b) SST $\kappa - \omega$, (c) $\gamma - \mathrm{Re}_\theta$ with $\nu_\tau/\nu = 2.5$ inflow condition, (d) $\gamma - \mathrm{Re}_\theta$ with $\nu_\tau/\nu = 10$ inflow condition. The colorbar ranges from -1.982e-01 to 1.177e+00.

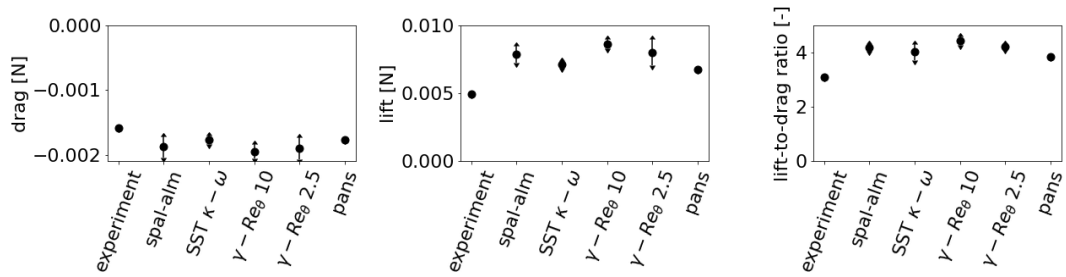

Fig. 7: Drag, lift and lift-to-drag ratio of experiments and numerical simulations. The values are taken from the finest grid setups and the error bars represent numerical uncertainty due to spatial discretisation. For experimental results the uncertainty is not give and for PANS is not computed yet.

We performed the SST $\kappa - \omega$ $\gamma - \mathrm{Re}_\theta$ simulations to test whether modelling of the transition to turbulent flow has a strong effect on the resultant aerodynamic forces on the wing. The results show that the transitional model gives values lying close the SST $\kappa - \omega$ without transition modelling ones (Figure 7), stating that the transitional model has a small impact on the results. Besides, Figure 5 corroborates such conclusion, since it shows that transition to turbulence takes place at almost the same point, roughly at 1/4 chord length for all the four setups. This is also confirmed by the velocity field, visible in Figure 6, which is characterised by separation on the leading edge followed by a separation bubble that sweeps the whole chord length and develops further in the wake.

PANS simulations were run with $f_k = 0.2$ and are the only ones to catch unsteadiness in the flow. The oscillations are mild though, ranging to a maximum of 3.5% of the mean values. It is important to underline that in PANS simulations, and in particular for a quite low f_k as 0.2, a conspicuous amount of turbulence is expected to be resolved. Therefore it is physically unlikely to obtain a smooth periodic solution: this suggests that the first three grids are inappropriate for the model, whilst the finest one could be the first one to provide plausible data. Since the size of the finest grid used is already significant, it is not within the means of this work to accomplish a full study with this model, which would result in heavy computational costs and efforts; therefore, PANS results reported here have to be considered as preliminary.

7 Conclusions

The present work shows a general schedule to approach the study of the airflow surrounding the wings of *Morpho* butterflies using computational fluid dynamics. Moreover, it provides a mathematical model for computing

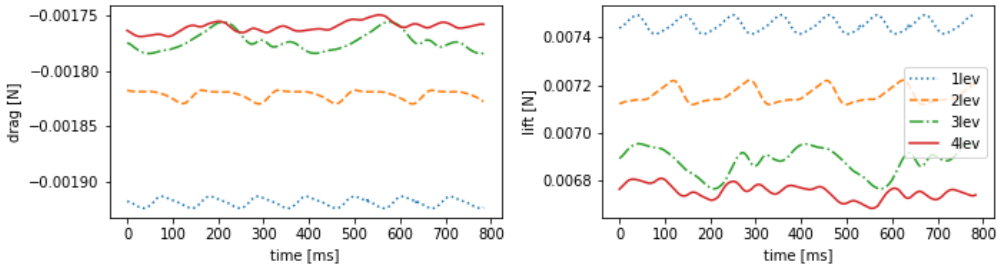

Fig. 8: Oscillatory aerodynamic forces for PANS simulations. Note that the coarser grids (1lev, 2lev, 3lev) provide periodical solutions, whilst the finest (4lev) provides a non periodical one.

the aerodynamic forces acting on a butterfly during gliding flight.

This study shows that, despite the strong assumptions and approximations made due to the limited tools available to study such delicate, small and light insects, numerical experiments can give results lying in the range of values indicated by experimental data.

The many different turbulence models used reveal concrete difficulties in catching the unsteady phenomena that experiments and previous literature suggest are taking place. Besides, $\kappa - \omega$ based models offer results that differ from each other by quantities that are consistently smaller than the ones between the experimental data and the numerical experiments themselves, stating how few the changes brought by transition modelling are. PANS simulations provide an interesting alternative surely capable to catch more detailed characteristics of the flow, even though this comes at a significant cost, which is perhaps unjustified considering the present setup, hypothesis, assumptions and uncertainties in the experimental data.

References

L. Eça and M. Hoekstra. A procedure for the estimation of the numerical uncertainty of CFD calculations based on grid refinement studies. *Journal of Computational Physics*, 262:104–130, 2014. ISSN 00219991. doi: 10.1016/j.jcp.2014.01.006. URL http://dx.doi.org/10.1016/j.jcp.2014.01.006.

R. B. Langtry and F. R. Menter. Transition Modeling for General CFD Application in Aeronautics. *43rd AIAA Aerospace Sciences Meeting and Exhibition*, pages 1–14, 2005.

F. R. Menter. Zonal Two Equation k-ω , Turbulence Models for Aerodynamic Flows . Florian R. Menter E. *24th Fluid Dynamics Conference July 6-9, 1993 / Orlando, Florida*, 1993.

F. R. Menter, R. B. Langtry, S. R. Likki, Y. B. Suzen, P. G. Huang, and S. VoÌlker. A Correlation-Based Transition Model Using Local Variables: Part I â Model Formulation. *Volume 4: Turbo Expo 2004*, (July):57–67, 2004. doi: 10.1115/GT2004-53452. URL http://proceedings.asmedigitalcollection.asme.org/proceeding.aspx?articleid=1638705.

S. P. Sane. The aerodynamics of insect flight. *Journal of Experimental Biology*, 206(23):4191–4208, 2003. ISSN 0022-0949. doi: 10.1242/jeb.00663. URL http://jeb.biologists.org/cgi/doi/10.1242/jeb.00663.

P. R. Spalart and S. R. Allmaras. A One-Equatlon Turbulence for Aerodynamic Flows. *30th Aerospace Sciences Meeting and Exhibit*, 1992.

G. R. Spedding, A. H. Hedenström, J. McArthur, and M. Rosén. The implications of low-speed fixed-wing aerofoil measurements on the analysis and performance of flapping bird wings. *Journal of Experimental Biology*, 211(2):215–223, 2008. ISSN 00220949. doi: 10.1242/jeb.007823.